Synthesis and Characterization of Molybdenum Incorporated Cubic Mesoporous Materials and the Study of Catalytic Activity of SBA-1 and MCM-48

Dhanju Mani Pathak[1,*,], Kishor Kr Shah[2,], Pankaj Kumar Ghosh[3,] and Anup Kumar Talukdar[4,]

[1]Department of Chemistry, Nalbari College, Nalbari-781335, India
[2]Department of Chemistry, A.D.P. College, Nagaon-782002, India
[3]Department of Chemistry, Mangaldai College, Darrang-784125, India
[4]Department of Chemistry, Gauhati University, Guwahati-781014, India

*Corresponding author: E-mail: dhanjumani@gmail.com

In present work, a two step synthetic procedure for the synthesis of MCM-48 materials is proposed. A sample of Mo-MCM-48 with Si/Mo ratio 100 was synthesized applying the same procedure as applied for the synthesis of Si-MCM-48 materials, only difference was that ammonium hepta-molybdate was added as a source of molybdenum in the second step. Two samples of SBA-1 and Mo-SBA-1 were also synthesized. The XRD patterns of synthesized Si-MCM-48 and Mo-MCM-48 and that of SBA-1 and Mo-SBA-1 were in good agreement with those of reported data for the cubic MCM-48 and SBA-1 materials. The synthesized samples were further characterized by FT-IR (for phase formation), TGA (for thermal stability), N_2 adsorption-desorption isotherm (for surface are, pore size and pore volume), UV-DRS (for insertion of Mo in the framework) and SEM (for morphology). The catalytic activity of synthesized MCM-48 was found to be better than SBA-1 for the esterification reaction of benzyl alcohol and acetic acid.

Keywords: Mesoporous materials, MCM-48, SBA-1, Esterification reaction.

INTRODUCTION

According to the International Union of Pure and Applied Chemistry (IUPAC), porous materials are classified into three classes based on their pore size; microporous (pore size < 2 nm), mesoporous (2-50 nm) and macroporous (> 50 nm) materials [1]. First mesoporous materials were synthesized in 1969 to overcome the pore size of microporous materials. However, because of lack of analysis, remarkable features of this meso-porous material were not recognized. One of the most exciting discoveries in the field of material engineering is the synthesis of a new family of mesoporous siliceous materials designated as M41S with exceptionally large and uniform pores by Mobil Oil Corporation research group in 1992 [2-4]. Large uniform pore sizes (1.5-10 nm), highly ordered nano channels, large surface areas (~1500 m²/g) and attractive liquid crystal structures are the desirable properties, which made such materials the focus of great interest [2,3,5]. There are three classes of M41S materials. These are MCM-41 (hexagonal, p6mm), MCM-48

(cubic, Ia3d) and MCM-50 (lamellar). MCM-41 has a hexa-gonal array of 1D pore system whereas the structure of MCM-48 is more complex than the former one having cubic symmetry with two intersecting unique 3D channel system. MCM-48 material is one member of the class M41S materials. Because of its cubic shape it is more attractive catalyst than MCM-41 materials. The cubic structure provides 3D channels, preventing them from being blocked by guest molecules, acts as catalyst support or adsorbent. Compared to one- or two-dimensional pore systems, the three-dimensional pore system of MCM-48 material has more resistance against pore blockage and provides a more efficient diffusion pathway. The important fact about the MCM-48 materials is that they possess long range ordered framework with uniform mesopores. By changing the synthesis conditions and/or by using surfactants with different chain lengths in their preparation, it is possible to adjust the pore size of the materials in the mesoporous range.

These materials also possess quite large surface area of the order of about 1000 m² g⁻¹. The synthesis process is quite

simple and by carefully adjusting the synthesis conditions, it is possible to synthesize hydrothermally stable MCM-48 mesoporous molecular sieve at extremely low cost using cetyltrimethylammonium bromide (CTAB). Further, it is possible to synthesize MCM-48 materials at lower surfactant (CTAB) concentration by increasing the crystallization temperature. Thus, during synthesis of MCM-48 materials, an increase in crystallization temperature from 373 K to 423 K can reduce the CTAB concentration from 0.65 to 0.1 of the CTAB/Si ratio. MCM-48 materials have found wide range of applications in various fields such as catalysts for various chemical reactions, as a support for drug delivery, *etc.*

The reported catalytic reactions using modified MCM-48 are oxidation of styrene by T-MCM-48 (T = Mn, V, Cr) [6], *tertiary* butylation of phenol by H-GaMCM-48 [7], 1-hexene hydroformylation by rhodium complexes ligated with triphenylphosphine analogs on amino-functionalized MCM-48 [8], photocatalytic reduction of CO_2 with H_2O on Ti-MCM-48 [9], acylation of anisole with octanyl chloride [10], synthesis of ε-caprolactam from cyclohexanone-oxime *via* Beckmann rearrangement over mesoporous molecular sieves MCM-48 [11], oxidative dehydrogenation of ethylbenzene in the presence of N_2O [12], phenol hydroxylation by CuO-containing MCM-48 [13], Fischer-Tropsch synthesis on MCM-48 supported cobalt [14], symmetric epoxidation of unfunctionalized olefins by Mn(III) salen complex immobilized on MCM-48 [15].

SBA-1 (Santa Barbara amorphous) having cubic phase with 3D-channel system with uniform pore structure is considered as suitable for catalyst support [16]. Huo *et al.* [16] reported that these SBA-1 materials are formed using combination of cationic surfactant (S+), halogen anion (X−) and silicate species (I+) through acidic route with high head group surfactant in pH range 1-2 [17]. Catalytic application of Mo-incorporated SBA-1 mesoporous molecular sieves to partial oxidation of methane [18] was reported. Cr–SBA-1 has been used as catalysts for dehydrogenation of ethane with carbon dioxide [19]. The 3D system of pores present in SBA-1 ensures easier accessibility of these pores to the reagent molecules than the 1D cylindrical pores, so SBA-1 has high application potential, for example, in adsorption and catalysis [20]. Mesoporous SBA-1 silicas have 3D cubic structure of *Pm*3*n* symmetry with open 3D cage type pores joined through open widows [21,22]. SBA-1 type materials show unique textural properties, including the quite high specific surface area in the range 1200-1450 m^2 g^{-1} and pore diameters varying from 2.1 to 2.6 nm. The 3D pore network is resistant to blocking and provides a large number of adsorption sites to the reactant molecules. Moreover, the pores are easily accessible to the reagents molecules [23,24]. Due to the textural parameters and high thermal stability, SBA-1 is considered as a good catalyst support [21]. Its cubic structure is more stable than that of the silicas of hexagonal structure (MCM-41 or SBA-15).

As molybdenum containing catalysts have the efficiency to catalyze a large number of reactions like hydrogenation, oxidation and metathesis reactions [25-27], so, Mo is chosen as an active metal in this study. Esterification of alcohols and carboxylic acids is one of the most fundamental organic transformations. Most of the esterification reactions were carried out in presence of sulphuric acid, hydrochloric acid and toxic materials, which are environmentally hazardous and unacceptable. Considering the impact of these chemicals on environment, MCM-48 and SBA-1 are used as acid catalyst in organic transformation. The use of MCM-48 and SBA-1 has great advantage because they can be reused. In the present study, cubic mesoporous MCM-48 and SBA-1 materials were synthesized and modified by incorporating Mo by *in situ* process. The catalytic activities of the synthesized mesoporous MCM-48 and SBA-1 materials are studied for the esterification reaction of benzyl alcohol and acetic acid.

EXPERIMENTAL

The materials used for the synthesis of MCM-48 and SBA-1 were cetyl trimethyl ammonium bromide (CTAB), tetraethyl orthosilicate (TEOS), sodium hydroxide (Merck), fumed silica (BDH and Fluka), HCl, ammonium heptamolybdate (Merck) and glycerol (Merck).

Synthesis of Si-MCM-48 materials: In present work, a two step process for the synthesis of MCM-48 materials were proposed. The MCM-48 structure was prepared according to the methodology reported in the literature [28].

Step-1: Preparation of surfactant solution: In this step, required amount of CTAB was dissolved in 91 mL of deionized water and to the solution 7.7 g of ethanol was added. The mixture was stirred for 15 min.

Step-2: Preparation of gel: In this step, a gel was prepared by dissolving 5 g of fumed silica in a NaOH solution with constant stirring. The gel was then stirred for 1 h.

The prepared gel was then added to the surfactant solution with constant stirring maintaining pH of 9.3. The mixture obtained was stirred for another 2 h to get a homogeneous composition. The whole mass was transferred to an autoclave and heated at 100 °C for 3 h and then at 150 °C for another 3 h. The solid product was then filtered, washed with hot water, dried at room temperature and then at 110 °C for 6 h. The sample was then calcined at 480 °C for 6 h in a muffle furnace. The gel composition for the synthesis of MCM-48 material is $Na_2O/SiO_2 = 0.21$, $CTAB/SiO_2 = 0.3$, $EtOH/SiO_2 = 5$ and H_2O/SiO_2 100.

Synthesis of Mo-MCM-48 materials: A sample of Mo-MCM-48 with Si/Mo ratio 100 was synthesized applying the same procedure as applied for the synthesis of Si-MCM-48 materials, ammonium heptamolybdate was added as a source of molybdenum in the second step. After crystallization, the same procedure stated above was applied for washing, drying and calcination.

Synthesis of SBA-1 material: Although we used the methodology presented in literature [29] for the synthesis of SBA-1, but the process was not used exactly and some modifications were made during its synthesis. In reported literature cetyl triethyl ammonium bromide (CTEAB) was used as surfactant, while in present work the cetyl trimethyl ammonium bromide (CTAB) was used as surfactant. In reported literature, glycerol was not used, while in the present work, glycerol is used. Because addition of glycerol as co-solvent offers an

effective synthetic approach for controlling the phase behaviour of cubic SBA-1 (*Pm3n* mesophase) over a broad temperature range [30].

Synthesis: About 9.1 g glycerol and surfactant (CTAB) were added with stirring to a HCl solution followed by the addition of 10.4 g TEOS with constant stirring. The mixture was stirred for 4 h at pH 2.1 and kept at room temperature for 1 day. After crystallization, it was filtered and washed with acetone to get contamination free solid product. This was dried at room temperature and then at 110 °C for 6 h. The sample was then calcined at 480 °C for 6 h in a muffle furnace. The gel composition and the conditions maintained for the synthesis of SBA-1 material is shown in Table-1. The novelty of the synthesis process is that it can be carried out at room temperature, while the reported synthesis process needs to reach to a temperature of 0 °C during its synthesis.

Synthesis of Mo-SBA-1 material: The same procedure was applied for synthesis of Mo-SBA-1 as mentioned for SBA-1. Only difference was that 1.543 g of ammonium heptamolybdate was added in the mixture, stirred for 4 h at room temperature and left for 1 day. After crystallization the solid product was recovered by filtration, which was washed with acetone. It was dried at room temperature and then at 110 °C for 6 h. The sample was then calcined at 480 °C for 6 h in a muffle furnace. The final gel composition is presented in Table-1.

Characterization: A Bruker D-8 Advance X-ray diffractometer with Cu*K*α radiation of wavelength 1.5418 Å operated at voltage = 40 kV and current = 40 mA was used for the X-ray powder diffraction analysis. The XRD patterns were taken in the 2θ = 5-50º with step size 0.05º and step time 0.5 s. Low angle X-ray powder diffraction patterns were obtained for the identification of mesoporous samples using a X'PERT PRO (Philips) diffractometer with Cu*K*α radiation of wavelength 1.54056 Å operated at a voltage 40 kV and current 30 mA. The XRD patterns were taken in the 2θ = 1.5-10º. A Perkin-Elmer RX 1 FTIR Spectrophotometer was used for recording the FT-IR spectra of the samples in the form of KBr pellets in mid-IR region of 4000-450 cm^{-1} (resolution 8 cm^{-1}). Thermogravimetric analysis (TGA) and differential thermal gravimetry (DTG) analysis of all the synthesized samples were done by using Mettler Toledo TGA/DSC 1, STAR^e system analyzer in the temperature range 313-1173 K with heating rate of 10 K min^{-1} in N_2 gas atmosphere. Diffuse reflectance UV-Vis spectra of the Mo incorporated samples were taken with a Hitachi 4100 spectrophotometer equipped with a diffuse reflectance attachment using solid sample holder in the range 200-800 nm at a scan speed of 600 nm min^{-1} (sampling interval: 2.00 nm). The base line correction was made using barium sulphate as the reference standard. For determining the specific surface area, pore volume and pore size of the synthesized samples a

Micromeritics (model: Tristar 3000) surface area and porosity analyzer was used. Prior to the experiments, all the samples were activated at 673 K for 2 h in high vacuum. After this treatment, liquid nitrogen was used to cool the samples to 74 K. The samples were allowed to adsorb nitrogen gas and complete isotherm was obtained (single point, P/P_0 = 0.13). BET surface was calculated using t-plot method and pore size distribution (PSD) was calculated using Barrett-Joyner-Halenda (BJH) formula. For the determination of particle morphology, scanning electron micrograph of the synthesized samples were taken by using LEO1430VP; Carl Zeiss scanning electron microscope and Hitachi, S-3600 N scanning electron microscope operating at accelerating voltage of 15-20 kV.

RESULTS AND DISCUSSION

XRD Studies: The XRD patterns of Si-MCM-48 and Mo-MCM-48 synthesized by two step process were in good agreement with those of reported data for the cubic MCM-48 materials [2,3]. The most distinguishable peak along (*211*) plane appears at 2θ = 2.7º and a shoulder peak at 3º which is for (*220*) plane. The XRD patterns of Si-MCM-48 and Mo-MCM-48 materials are shown in Fig. 1. It is evident that *211* peak for Mo-MCM-48 shifts towards lower 2θ value in comparison to that of Si-MCM-48. Such a shift of *211* peak towards lower 2θ values, is an indication of successful incorporation of Mo into the framework of MCM-48 [33].

The XRD patterns of SBA-1 and Mo-SBA-1 materials are shown in Fig. 2. From the XRD patterns of SBA-1 and
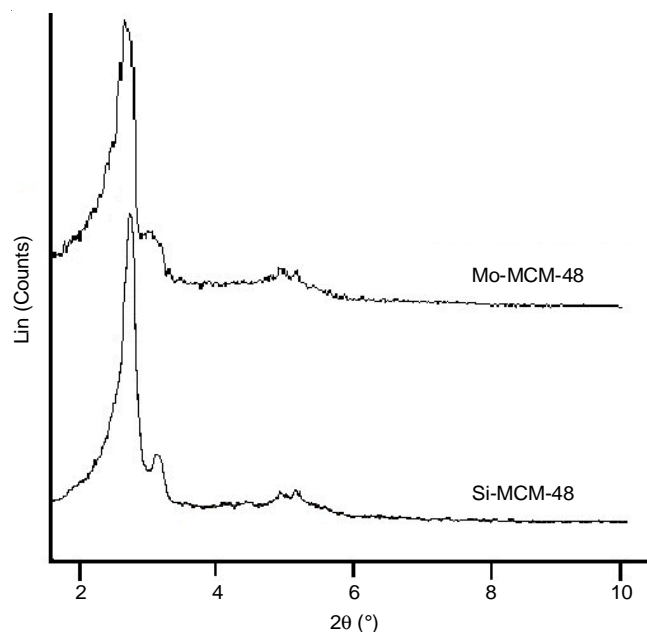

Fig. 1. XRD patterns of Si-MCM-48 and Mo-MCM-48

TABLE-1
GEL COMPOSITION OF SBA-1 AND Mo-SBA-1

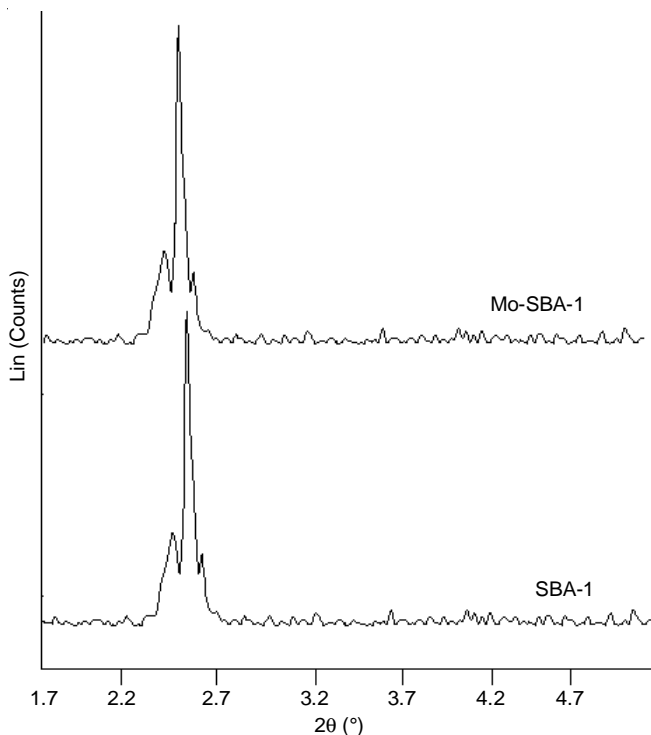| Samples designation	Silica source	CTAB/SiO$_2$	HCl/SiO$_2$	EtOH/SiO$_2$	H$_2$O/SiO$_2$	pH of the gel	Ammonium heptamolybdate/SiO$_2$
SBA-1	TEOS	0.2	40	2	150	2.1	–
Mo-SBA-1	TEOS	0.2	40	2	150	2.4	0.025

Fig. 2. XRD pattern of SBA-1 and Mo-SBA-1

Fig. 4. FT-IR spectra of Mo-MCM-48

Mo-SBA-1, it is evident that *211* peak for Mo-SBA-1 shifts towards lower 2θ value in comparison to that of the SBA-1. Such a shift of *211* peak towards lower 2θ values, is an indication of successful incorporation of Mo into the framework of SBA-1 [31].

FT-IR studies: FT-IR spectra of Si-MCM-48 and Mo-MCM-48 are shown in Figs. 3 and 4, respectively. For both the samples the bands at 3500 cm^{-1} (broad) and at 1630 cm^{-1} are attributed to stretching and bending mode of water [32], respectively. On the other hand, the broad band at ~ 1084 cm^{-1} and shoulder band at wave-numbers ~1234 cm^{-1} and ~ 810 cm^{-1} are attributed to Si-O-Si asymmetric stretching and Si-O-Si bending vibrations, respectively [33-35].
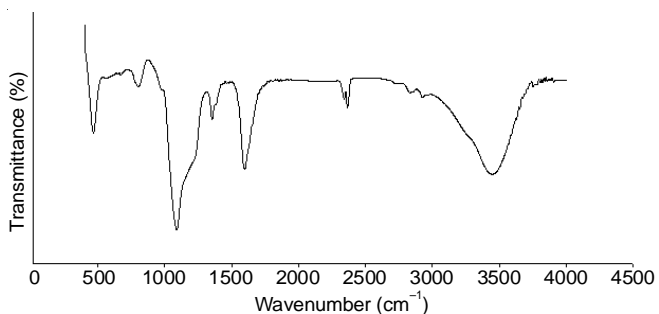

Fig. 3. FT-IR spectra of Si-MCM-48

The FT-IR spectra of SBA-1 and Mo-SBA-1 materials are shown in Fig. 5. In the spectra, the band at ~ 3500 cm^{-1} may be assigned to the O-H stretching vibration of the silanol groups. The band at ~ 1635 cm^{-1} may be assigned to the H-O-H bending vibration of water molecule. The bands at ~ 1000, ~ 780 and ~ 540 cm^{-1} may be assigned to Si-O asymmetric stretching, Si-O symmetric stretching and Si-O-Si bending vibrations,

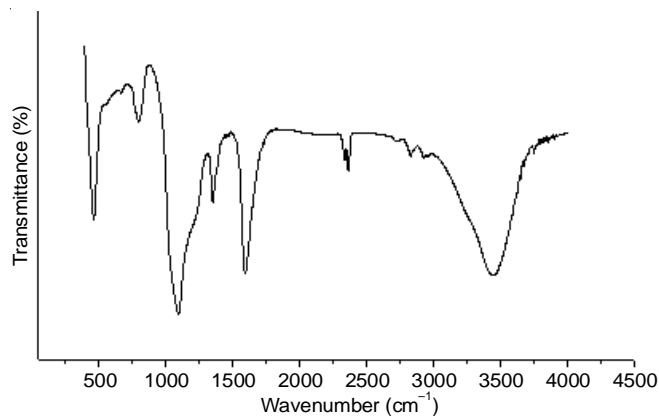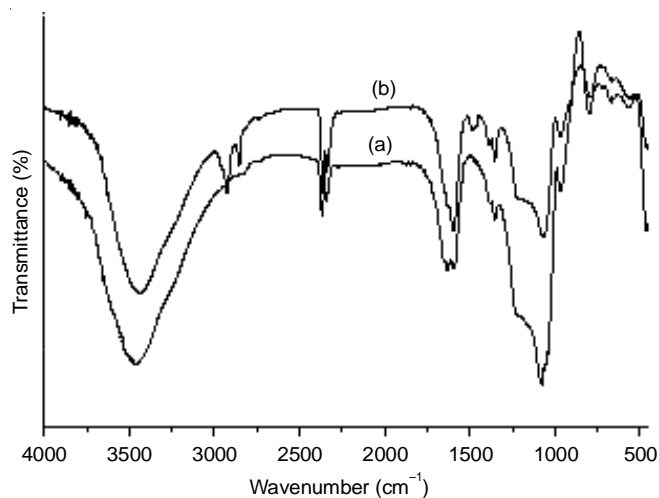Fig. 5. FT-IR spectra of (A) SBA-1 and (B) Mo-SBA-1

respectively [36]. From the XRD and FT-IR analysis, it can be concluded that MCM-48 and SBA-1 were successfully synthesized.

SEM studies: The SEM micrographs of Si-MCM-48 and Mo-MCM-48 are shown in Figs. 6 and 7. It is seen that quite uniform cubical shaped particles were formed and the size of the particles was found to be nearly 0.5 µm. The morphology of the MCM-48 samples remained unchanged even on Mo incorporation. The SEM micrograph of SBA-1 is shown in Fig. 8. The SEM images are spherical in nature. The particle size of SBA-1 ranges from 5 to 7 µm.

Thermal studies: The TGA curves of Si-MCM-48 and Mo-MCM-48 are shown in Figs. 9 and 10, respectively. It is found that on heating Si-MCM-48 sample show weight loss at four temperature ranges 323-424 K, 425-523 K, 524-655 K and finally 656-1013 K, while Mo-MCM-48 sample show weight loss at five temperature ranges 323-424 K, 425-523 K, 524-655 K, 656-775 K and finally 776-1013 K. The initial weight loss in the temperature range 323-424 K is due to the loss of physically adsorbed water molecule [37]. The template loss in case of Si-MCM-48 takes place in two temperature ranges *i.e.* in 425-523 K and 524-655 K, while the template loss in case of Mo-MCM-48 takes place in three temperature ranges *i.e.* in 425-523 K, 524-655 K and 656-775 K. The weight loss in the temperature range 656-1013 K (for Si-MCM-48) and

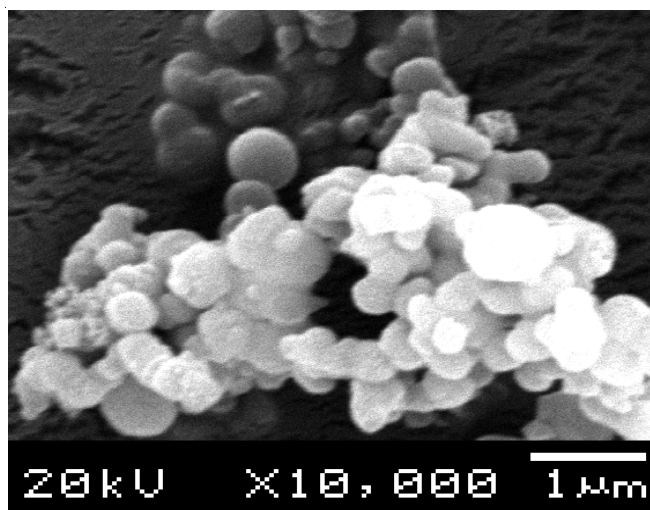Fig. 6. SEM image of Si-MCM-48

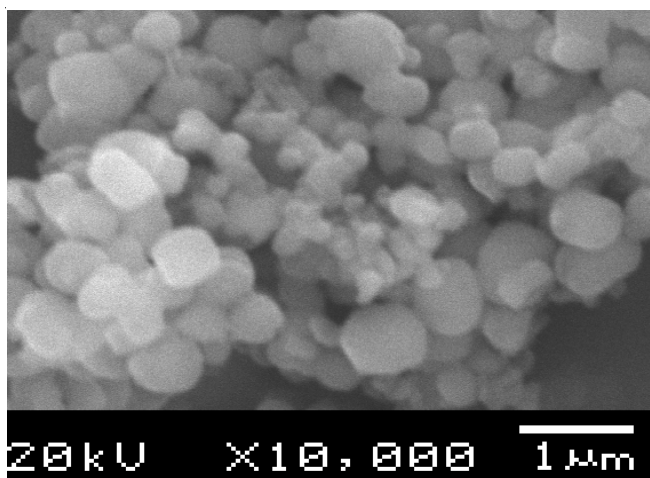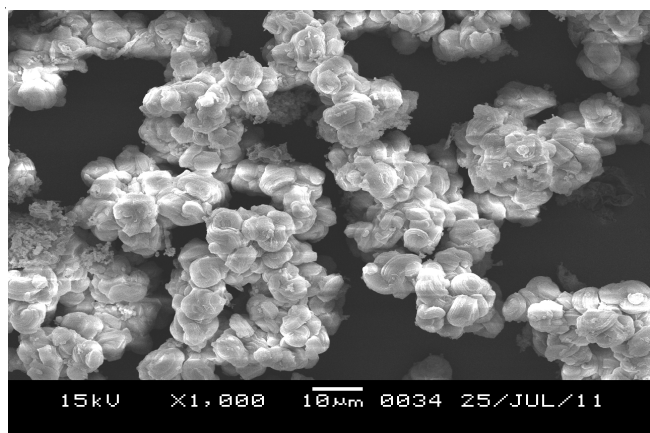Fig. 9. TGA graph of Si-MCM-48
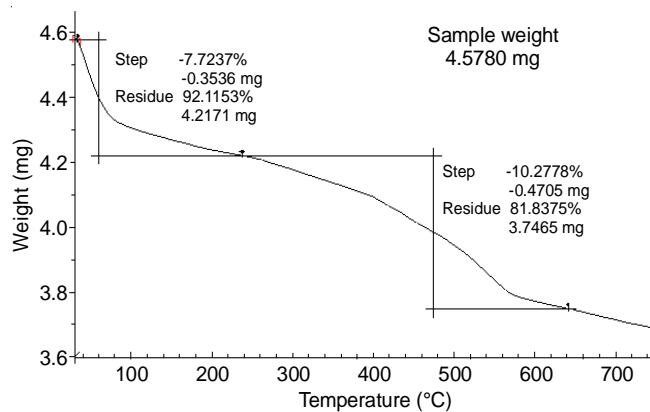

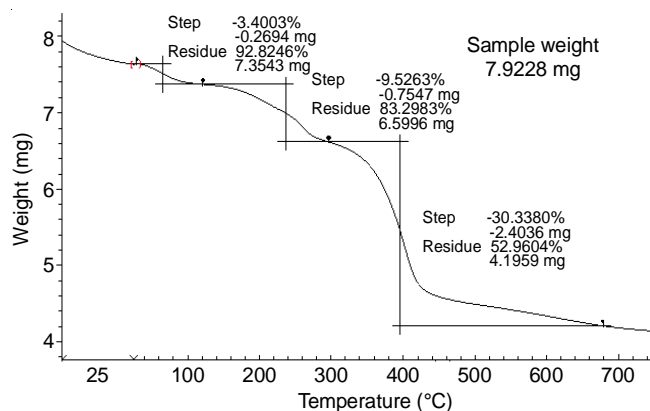Fig. 7. SEM image of Mo-MCM-48

Fig. 10. TGA graph of Mo-MCM-48

Fig. 8. SEM micrograph of SBA-1

776-1013 K (for Mo-MCM-48) may be attributed to the loss of CTAB surfactant bound strongly inside the channels. The percentage of weight loss is found to be increased as molybdenum is introduced in the MCM-48 samples. The mass % loss at different ranges of temperatures for the synthesized samples is shown in Table-2.

Adsorption-desorption studies: The N_2 adsorption-desorption isotherms of Si-MCM-48 and Mo-MCM-48 samples are shown in Figs. 11 and 12 respectively, which, indicate that the isotherms are of type IV, typical for mesoporous solids [38]. Pore size distributions of MCM-48 materials were obtained from the adsorption data by means of the Barrett-Joyner-Halenda (BJH) formula [39]. The BET surface area, pore volume and pore diameter of MCM-48 materials are listed in Table-3. From this study, it is clear that with the incorporation of Mo, the BET surface area decreases from 683.81 m^2 g^{-1} (for Si-MCM-48) to 620.16 m^2 g^{-1} (for Mo-MCM-48). On the other hand, BJH pore diameter and pore volume increases from 24.9 Å (for Si-MCM-48) to 41.5 Å (for Mo-MCM-48) and 0.22 cm^3 g^{-1} (for Si-MCM-48) to 0.30 $cm^3 g^{-1}$ (for Mo-MCM-48), respectively.

TABLE-2
MASS % LOSS OF Si-MCM-48 AND Mo-MCM-48 AT DIFFERENT TEMPERATURE RANGE

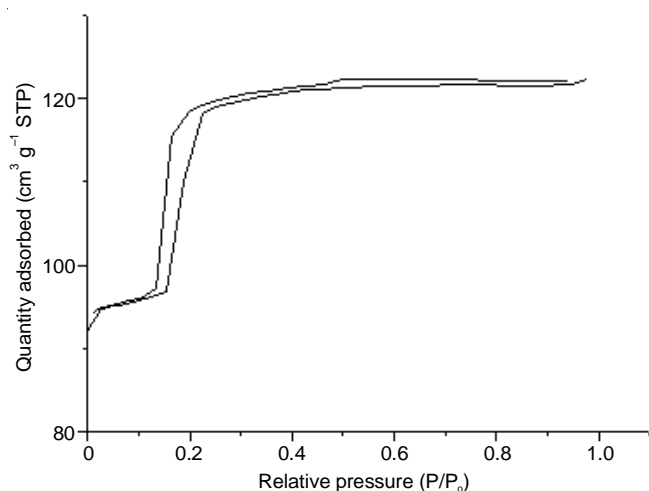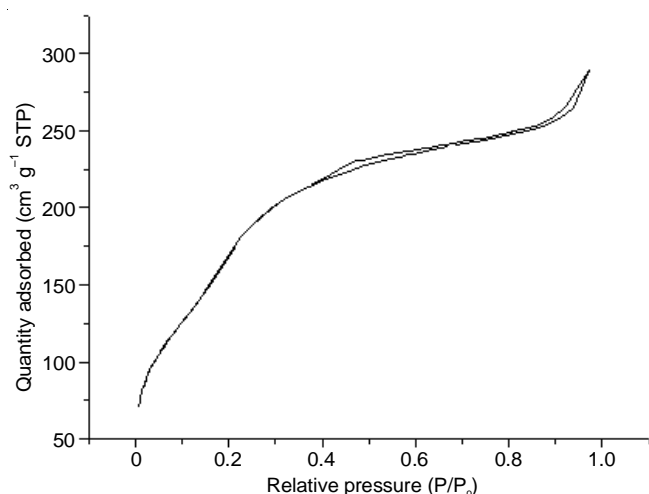| Sample	Mass percentage loss in temperature ranges (K)				
	323-424	425-523	524-655	656-1013	Total
Si-MCM-48	2.2	7.6	9.6	3.2	22.6
Mo-MCM-48	2.8	24.1	11.3	4.7 (656-775K) 6.9 (776-1013K)	49.8

Fig. 11. N$_2$ adsorption-desorption curve of Si-MCM-48

Fig. 12. N$_2$ adsorption-desorption curve of Mo-MCM-48

TABLE-3
BET SURFACE AREA, PORE VOLUME AND
PORE DIAMETER OF MCM-48 MATERIALS

| Samples | Physical properties | | |
	BET surface area (m^2 g^{-1})	BJH adsorption average pore diameter (Å)	BJH desorption cumulative pore volume (cm^3 g^{-1})
Si-MCM-48	683.81	24.9	0.22
Mo-MCM-48	620.16	41.5	0.30

UV-DRS studies: The UV-DR spectroscopy is a very sensitive technique for the determination of coordination of metal ion in the framework or extra framework position in metal containing mesoporous materials [40]. The diffuse reflectance UV-visible spectroscopy was used to know the coordination of metal ion in Mo-MCM-48 material and the spectrum is shown in Fig. 13. The absorption bands at 250 and 330 nm are observed in the UV-visible spectra of Mo-MCM-48 samples, which are for the tetra- and hexa-coordinated Mo^{6+} cation, respectively. Oxo-molybdenum compounds give absorption bands in UV-visible region due to ligand-metal charge transfer (O^{2-}-Mo^{6+}). The position of this electronic transition depends on the ligand field symmetry surrounding the Mo center; the tetrahedral Mo^{6+}(T$_d$) is expected to show a higher energy
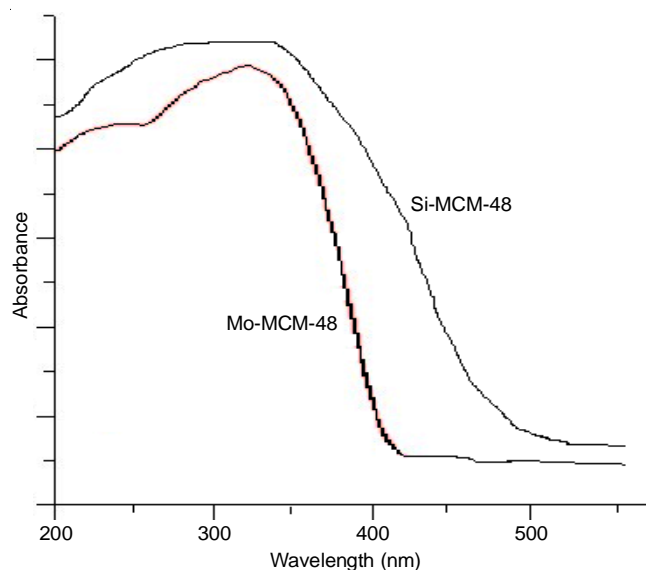

Fig. 13. UV- Vis (DRS) spectrum of Si-MCM-48 and Mo-MCM-48

transition than for the octahedral one [41]. Absorption bands around 230 nm may be due to the contributions of octahedral and tetrahedral Mo^{6+}. Bands from 250 to 280 nm have been assigned to Mo^{6+} {T$_d$(t$_1$-e)} and bands from 300 to 330 nm to Mo^{6+} (O$_h$(t$_{2u}$,t$_{1g}$- t$_{2g}$)) [42]. These bands were quite broad in case of Si-MCM-48, as is evident from Fig. 13. The absorbance bands at wavelength ~ 250 nm and ~ 330 nm may be assigned to the incorporation of Mo in MCM-48 framework.

Catalytic activity: In organic synthesis, the esterification reaction is one of the fundamental reactions and has great use [43]. In present study, esterification reaction of benzyl alcohol and acetic acid is studied using modified MCM-48 and SBA-1 catalysts. Benzyl acetate is the major product of this reaction. The reaction is shown in **Scheme-I**.
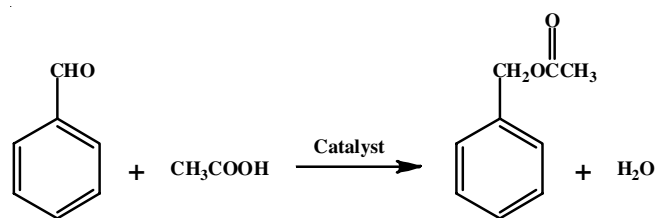
Scheme-I: Esterification reaction of benzyl alcohol and acetic acid

The reactions were carried out in glass batch reactor under atmospheric pressure. The temperature of the reaction was controlled by a temperature controller and stirring was done by a magnetic stirrer. Before the use of catalysts in the reaction, it was activated by heating at 373 K temperature for 4 h. In order to study the catalytic activity of the synthesized samples, a fixed volume of the reaction mixture was taken out at regular interval of time and is put in a beaker containing ice to freeze the reaction. The product and the unreacted reactants of the reaction mixture, collected at different time intervals, were analyzed by gas chromatography (Perkin-Elmer, Clarus 500, Elite 501 column). From the results obtained, the percentage conversions under different reaction conditions were calculated.

The effect of temperature on the esterification reaction of benzyl alcohol was studied in the temperature range of 343 K to 383 K using SBA-1 and MCM-48. The reaction was carried out under atmospheric pressure taking 0.2 g catalyst with reactant mixture in 1:2 molar ratio. The conversion of benzyl alcohol at different temperatures for reaction time of 8 h using catalysts SBA-1 and MCM-48 is shown in Table-4. The conversion of benzyl alcohol is found to increase with increase in temperature. No side product was obtained up to 383 K, which indicates the absence of dehydration of Friedel-Craft acylation. There was a sharp increase of conversion of benzyl alcohol from 40.4% to 58.9% and from 45.6% to 59.1%, when temperature was increased from 343 K to 373 K for SBA-1 and MCM-48, respectively. When the temperature was increased further to 383 K, the reaction slowed down for both the catalysts. This may be due to the blockage of adsorption sites of the catalysts at higher temperature. Thus, the temperature 373 K may be considered as the optimum temperature for the esterification of benzyl alcohol.

TABLE-4
EFFECT OF TEMPERATURE ON THE ESTERIFICATION
REACTION ON SBA-1 AND MCM-48

Temperature (K)	Catalyst	Conversion (%)
343	SBA-1	40.4
	MCM-48	45.6
373	SBA-1	57.8
	MCM-48	58.1
383	SBA-1	58.9
	MCM-48	59.1

Time = 8 h, Catalyst amount = 0.2 g, Benzyl alcohol: acetic acid = 1:2 (molar ratio), Substrate volume = 16 mL.

The effect of amount of catalyst on the esterification reaction of benzyl alcohol was studied by taking 0.2 and 0.4 g of each of SBA-1 and MCM-48. The reactions were done under atmospheric pressure and at 373 K with reactant mixture in 1:2 molar ratio. The conversion of benzyl alcohol with different amount of catalyst for reaction time 8 h is shown in Table-5 for catalysts SBA-1 and MCM-48. It has been previously investigated that the conversion of benzyl alcohol in esterification reaction over heterogeneous catalysts does not depend upon the total number of acid sites of the catalysts [44]. That is why, the effect of pore size and surface area on the conversion of this esterification reaction was also studied. Mesoporous materials have high surface area. It is indicated that there is a combined effect of pore size and surface area on the different conversions of benzyl alcohol under similar reaction conditions. The conversion of benzyl alcohol slightly increases with increase

TABLE-5
EFFECT OF AMOUNT OF CATALYST ON THE
ESTERIFICATION REACTION OVER DIFFERENT CATALYSTS

Catalyst amount (g)	Conversion (%)	
	SBA-1	MCM-48
0.2	57.8	58.1
0.4	59.7	60.4

Time = 8 h, Temperature = 373 K, Benzyl alcohol: acetic acid = 1:2 (molar ratio), Substrate volume: 16 mL, Catalyst amount: 0.2 and 0.4 g

in the amount of catalyst. This is due to the reversibility of the esterification reaction [44]. No side product is obtained at this temperature and 10 h duration time. Thus, 100% selectivity towards the formation of benzyl acetate can be obtained.

The effect of alcohol and acid molar ratio on the esterification reaction of benzyl alcohol was studied by taking 1:2 and 2:1 molar ratio of the reactants and 0.2 g of each of SBA-1 and MCM-48. The reaction was carried out under atmospheric pressure at 373 K. The conversion of benzyl alcohol at different molar ratios for reaction time 8 h is shown in Table-6 for catalysts SBA-1 and MCM-48. The conversion of benzyl alcohol increased with increase in the amount of acetic acid in the reaction mixture. This is due to the fact that there was a competition between benzyl alcohol and acetic acid for adsorption on the catalyst surface. Thus, for esterification reaction, acid adsorption was necessary in the surface of catalyst [45]. Also, when acetic acid concentration is more in the reactants, the competitive adsorption of the acid on the surface was obviously more facilitating the esterification reaction to proceed at faster rate. On the other hand, if alcohol concentration was more in the reaction mixture, there was a possibility of saturation of the surface with alcohol blocking the acid adsorption [44]. The esterification reaction in the present study took place between the adsorbed acid on the catalysts surface, which formed an electrophile and benzyl alcohol. Therefore, the efficiency of the catalyst in this reaction is depended on the ability to adsorb the alcohol, which will hinder the reaction. No side product was obtained at this temperature and 8 h duration time. Thus 100% selectivity towards the formation of benzyl acetate can be obtained.

TABLE-6
EFFECT OF MOLAR RATIO ON THE ESTERIFICATION
REACTION OVER DIFFERENT CATALYSTS

Molar ratio (benzyl alcohol: acetic acid)	Conversion (%)	
	SBA-1	MCM-48
1:2	57.8	58.1
2:1	57	57.5

Time = 8 h, Temperature = 373 K, Catalyst amount= 0.2 g, Substrate volume: 16 mL.

Conclusion

From the XRD and FT-IR analysis, it is observed that MCM-48 and SBA-1 were successfully synthesized and molybdenum was incorporated in the MCM-48 materials. The SEM images indicated that the materials were spherical in nature. The particle size of SBA-1 ranges from 5 to 7 µm. The esterification reaction of benzyl alcohol with acetic acid was carried out successfully at temperature range 343 K to 383 K over the catalysts SBA-1 and MCM-48. The reaction was studied under different conditions such as temperature, catalyst amount and reactants molar ratio. Under all the conditions the selectivity of benzyl acetate is 100% and no side product is obtained under any conditions. The conversion (%) of benzyl acetate increases with increase in reaction time, temperature and catalyst amount. However, the temperature 373 K may be considered as the optimum temperature for the said reaction, as above this temperature the increase in % conversion is not significant. The

conversion of benzyl alcohol increased with increase in the amount of acetic acid in the reaction mixture. But the conversion (%) decreases with increase in benzyl alcohol concentration. The activity of MCM-48 catalyst on the esterification reaction was found to be more than that of SBA-1. As the esterification reaction is an acid catalyzed reaction, so, it is concluded that surface acidity of MCM-48 is more than that of SBA-1. The novelty of the present work is that Mo was successfully incorporated in the framework of MCM-48 and SBA-1. The synthesis process for SBA-1 can be carried out at room temperature in contrast to that of the already reported process that needs to reach to a temperature of 0 ℃ during its synthesis. Both the catalysts were found to be quite efficient for the esterification reaction. The % conversion was found to be 58.9 and 59.1 with SBA-1 and MCM-48, respectively.

ACKNOWLEDGEMENTS

CONFLICT OF INTEREST

The authors declare that there is no conflict of interests regarding the publication of this article.

REFERENCES

1. K.S.W. Sing, D.H. Everett, R.A.W. Haul, L. Moscou and R.A. Pierotti, *Pure Appl. Chem.*, **57**, 603 (1985);
    https://doi.org/10.1351/pac198557040603
2. C.T. Kresge, M.E. Leonowicz, W.J. Roth, J.C. Vartuli and J.S. Beck, *Nature*, **359**, 710 (1992);
    https://doi.org/10.1038/359710a0
3. J.S. Beck, J.C. Vartuli, W.J. Roth, M.E. Leonowicz, C.T. Kresge, K.D. Schmitt, C.T.W. Chu, D.H. Olson, E.W. Sheppard, S.B. McCullen, J.B. Higgins and J.L. Schlenker, *J. Am. Chem. Soc.*, **114**, 10834 (1992);
    https://doi.org/10.1021/ja00053a020
4. J.C. Vartuli, C.T. Kresge, M.E. Leonowicz, A.S. Chu, S.B. McCullen, I.D. Johnson and E.W. Sheppard, *Chem. Mater.*, **6**, 2070 (1994);
    https://doi.org/10.1021/cm00047a029
5. T. Yanagisawa, T. Shimizu, K. Kuroda and C. Kato, *Bull. Chem. Soc. Jpn.*, **63**, 988 (1990);
    https://doi.org/10.1246/bcsj.63.988
6. S. Gómez, L.J. Garces, J. Villegas, R. Ghosh, O. Giraldo and S.L. Suib, *J. Catal.*, **233**, 60 (2005);
    https://doi.org/10.1016/j.jcat.2005.04.015
7. S.E. Dapurkar and P. Selvam, *J. Catal.*, **224**, 178 (2004);
    https://doi.org/10.1016/j.jcat.2004.02.033
8. Q. Peng, Y. Yang and Y. Yuan, *J. Mol. Catal. Chem.*, **219**, 175 (2004);
    https://doi.org/10.1016/j.molcata.2004.05.003
9. M. Anpo, H. Yamashita, K. Ikeue, Y. Fujii, S.G. Zhang, Y. Ichihashi, D.R. Park, Y. Suzuki, K. Koyano and T. Tatsumi, *Catal. Today*, **44**, 327 (1998);
    https://doi.org/10.1016/S0920-5861(98)00206-5
10. P.C. Shih, J.H. Wang and C.Y. Mou, *Catal. Today*, **93**, 365 (2004);
    https://doi.org/10.1016/j.cattod.2004.06.025
11. J.C. Chang and A.N. Ko, *Catal. Today*, **97**, 241 (2004);
    https://doi.org/10.1016/j.cattod.2004.07.010
12. P. Kuœtrowski, L. Chmielarz, J. Surman, E. Bidziñska, R. Dziembaj, P. Cool and E.F. Vansant, *J. Phys. Chem. A*, **109**, 9808 (2005);
    https://doi.org/10.1021/jp0535442
13. L.L. Lou and S. Liu, *Catal. Commun.*, **6**, 762 (2005);
    https://doi.org/10.1016/j.catcom.2005.07.004
14. H. Li, S. Wang, F. Ling and J. Li, *J. Mol. Catal. Chem.*, **244**, 33 (2006);
    https://doi.org/10.1016/j.molcata.2005.08.050
15. K. Yu, L.L. Lou, C. Lai, S. Wang, F. Ding and S. Liu, *Catal. Commun.*, **7**, 1057 (2006);
    https://doi.org/10.1016/j.catcom.2006.05.017
16. Q. Huo, D.I. Margolese, U. Ciesla, P. Feng, T.E. Gier, P. Sieger, R. Leon, P.M. Petroff, F. Schüth and G.D. Stucky, *Nature*, **368**, 317 (1994);
    https://doi.org/10.1038/368317a0
17. M.S. Morey, A. Davidson and G.D. Stucky, *J. Porous Mater.*, **5**, 195 (1998);
    https://doi.org/10.1023/A:1009626103498
18. L.X. Dai, Y.H. Teng, K. Tabata, E. Suzuki and T. Tatsumi, *Micropor. Mesopor. Mater.*, **44-45**, 573 (2001);
    https://doi.org/10.1016/S1387-1811(01)00236-0
19. X. Zhao and X. Wang, *J. Mol. Catal. A*, **261**, 225 (2007);
    https://doi.org/10.1016/j.molcata.2006.08.008
20. M.C. Liu, H.S. Sheu and S. Cheng, *Chem. Commun.*, **23**, 2854 (2002);
    https://doi.org/10.1039/b209009k
21. S. Jarmoliñska, A. Feliczak-Guzik and I. Nowak, *Materials*, **13**, 4385 (2020);
    https://doi.org/10.3390/ma13194385
22. Y. Sakamoto, M. Kaneda, O. Terasaki, D.Y. Zhao, J.M. Kim, G. Stucky, H.J. Shin and R. Ryoo, *Nature*, **408**, 449 (2000);
    https://doi.org/10.1038/35044040
23. P. Srinivasu and A. Vinu, *Chem. Eur. J.*, **14**, 3553 (2008);
    https://doi.org/10.1002/chem.200701946
24. P. Michorczyk, J. Ogonowski and M. Niemczyk, *Appl. Catal. A Gen.*, **374**, 142 (2010);
    https://doi.org/10.1016/j.apcata.2009.11.040
25. E.A. Lombardo, M.L. Jacono and W.K. Hall, *J. Catal.*, **64**, 150 (1980);
    https://doi.org/10.1016/0021-9517(80)90488-1
26. G.W. Keulks, *J. Catal.*, **19**, 232 (1970);
    https://doi.org/10.1016/0021-9517(70)90287-3
27. J.J. Rooney and A. Stewart, *Chem. Soc. Spec. Period. Rep. Catal.*, **1**, 277 (1977).
28. B. Kalita, P. Phukan and A.K. Talukdar, *Catal. Sci. Technol.*, **2**, 2341 (2012);
    https://doi.org/10.1039/C2CY20198D
29. G. Imran and R. Maheswari, *Mater. Chem. Phys.*, **161**, 237 (2015);
    https://doi.org/10.1016/j.matchemphys.2015.05.043
30. H.M. Kao, C.C. Cheng, C.C. Ting and L.Y. Hwang, *J. Mater. Chem.*, **15**, 2989 (2005);
    https://doi.org/10.1039/b504320d
31. K.K. Shah, J. Saikia, D. Saikia and A.K. Talukdar, *Mater. Chem. Phys.*, **134**, 43 (2012);
    https://doi.org/10.1016/j.matchemphys.2012.02.012
32. L.H. Little, Infrared Spectra of Adsorbed Species, Academic Press: London (1966).
33. W. Zhan, G. Lu, Y. Guo, Y. Guo, Y. Wang, Y. Wang, Z. Zhang and X. Liu, *J. Rare Earths*, **26**, 515 (2008);
    https://doi.org/10.1016/S1002-0721(08)60129-5
34. A.A. Romero, M.D. Alba and J. Klinowski, *J. Phys. Chem. B*, **102**, 123 (1998);
    https://doi.org/10.1021/jp971469s
35. F.L. Galeener, A.J. Leadbetter and M.W. Stringfellow, *Phys. Rev. B Condens. Matter*, **27**, 1052 (1983);
    https://doi.org/10.1103/PhysRevB.27.1052
36. S. Molaei, T. Tamoradi, M. Ghadermazi and A.G. Choghamarani, *Appl. Organomet. Chem.*, **33**, e4977 (2019);
    https://doi.org/10.1002/aoc.4977
37. K.K. Shah, M. Nandi and A.K. Talukdar, *Mater. Res. Bull.*, **66**, 101 (2015);
    https://doi.org/10.1016/j.materresbull.2015.01.018
38. S. Brunauer, L.S. Deming, W.S. Deming and E. Teller, *J. Am. Chem. Soc.*, **62**, 1723 (1940);
    https://doi.org/10.1021/ja01864a025
39. E.P. Barrett, L.G. Joyner and P.P. Halenda, *J. Am. Chem. Soc.*, **73**, 373 (1951);
    https://doi.org/10.1021/ja01145a126
40. J. Xu, Z. Luan, H. He, W. Zhou and I. Kevan, *Chem. Mater.*, **10**, 3690 (1998);
    https://doi.org/10.1021/cm980440d
41. R.S. Weber, *J. Catal.*, **151**, 470 (1995);
    https://doi.org/10.1006/jcat.1995.1052
42. C.C. Williams, J.G. Ekerdt, J.M. Jehng, F.D. Hardcastle, A.M. Turek and I.E. Wachs, *J. Phys. Chem.*, **95**, 8781 (1991);
    https://doi.org/10.1021/j100175a067
43. R.C. Larock, Comprehensive Organic Transformations, VCH Publishers: New York, Chap. 9 (1989).
44. J. D'Souza and N. Nagaraju, *Indian J. Chem. Technol.*, **13**, 60 (2006).
45. S.R. Kirumakki, N. Nagaraju and S. Narayanan, *Appl. Catal.*, **273**, 1 (2004);
    https://doi.org/10.1016/j.apcata.2004.03.016